



Impact of Environmental Conditions on Rammed Earth Heritage Buildings Seismic Performance

J. Villacreses¹, B. Caicedo², and F. Yépez¹ (✉)

¹ College of Science and Engineering, Universidad San Francisco de Quito USFQ, Quito 170901, Ecuador
fyopez@usfq.edu.ec

² Universidad de los Andes, 111711 Bogotá, Colombia

Abstract. Heritage buildings in high seismic hazard areas usually have high vulnerability due to many factors affecting their seismic performance, including material properties, construction procedures applied and preservation conditions. One especially vulnerable structural system used for thousands of years, is the one using compacted soils as a construction material, called rammed earth structure. As rammed earth walls dry and harden, material properties and strength increases. However, weather phenomena during time like storms, floods, ice and snow change walls water content and could change overall structural behavior if there is no protection covers over walls. The aim of this work is to analyze the influence of weather on the seismic performance of rammed earth walls. Water content profiles of two selected walls were calculated and evaporation flux was modelled from experimental data in reduced scale models inside a climatic chamber. After, a finite element model was used for computing dynamic linear and nonlinear performance of earthen walls subjected to selected strong motion records, in different weather conditions. Results indicated that wall shear modulus increase as matric soil suction increase, rising earthen wall's stiffness in dry conditions, increasing vibration frequencies. Under different water content situations, wall's stiffness change, vibration frequencies decay and seismic performance changes considerably. Nonlinear walls' behaviour indicates variable differences between dynamic results under saturation and under residual dry conditions. Those differences will have considerable impact in the design, construction, strengthening or rehabilitation programs on rammed earth buildings, impact that has been neglected when considering earthquake resistance and vulnerability of heritage constructions.

Keywords: Rammed earth walls · weather impact · seismic performance · matric soil suction · pesidual dry conditions

1 Introduction

Compacted soils have been used as a construction material for buildings (called earthen structures) for thousands of years [1]. The main three types of such structures are masonry block, cob and rammed earth wall structures [2]. Rammed earth structures are made using

compacted soil in layers inside a formwork for building structural wall members [3, 4]. Optimum soil water content and density are commonly used as reference parameters for construction when they are engineered. Many of this type of buildings have historical and heritage value; therefore, it is important to understand which will be their future structural performance, especially when they are in high seismic hazard areas, in order to design and to execute strengthening programs for heritage conservation.

Any earthen structure can be affected by water content, especially if structures are not covered by any damp-proof cover. Water content has a remarkable impact on soil resistance [5–7]. The degree of saturation modifies water pressures inside the soil skeleton, causing changes in the stress state and the elastic material properties [8]. Changes in pore water pressure, can affect structural stiffness and wall's structural performance. François et al. [9] investigated the structure strength evolution of an earthen wall as a function of the relative humidity under axial loading, showing that the increase in water content produces additional deformations in the structure induced by loading conditions. In the same way, weather conditions can affect structural characteristics of rammed earth structures. Water content within soil walls changes since the beginning of the construction stage and during the structure's life service. Evaporation in dry seasons and wetting in rainy seasons will change pore water pressure inside the earthen structural elements, affecting building overall structural behavior under loads. There is a lack of investigation regarding the influence of such water content changes and seismic behavior of rammed earth walls. The aim of this paper is to contribute to the knowledge in this area.

2 Walls, Materials, Methods and Models

Two earthen walls having 2.5 m length, 2.4 m height and two different thicknesses (0.30 and 0.50 m) were selected, based on the studies conducted by Bui et al. and El-Nabouch et al. [10–15]. Fine-grained compacted soil (high plasticity clay CH) with 87% liquid limit and 37% plastic limit were the selected materials, compacted to a optimum density (1.34 g/cm^3) and optimum water content (31.4%) according to the ASTM D698 Proctor Standard Optimal Test.

Soil dynamic parameters were studied before, using a dynamic shear rheometer applying a torsional deformation control procedure that allows measuring the maximum shear modulus and the shear modulus degradation curve in samples conditioned to different saturation degrees, therefore, to different suction values and for a range of shear strains from 1×10^{-5} to 1×10^{-3} (Fig. 1) [16]. From the same test, experimental results relating saturation and suction can be observed in Fig. 1 and a comparison with the fitting curve proposed by Fredlung & Xing [17]. Upper value indicates the air entry representing the pore pressure where air starts to enter the soil skeleton's large pore space. Lower value shows the residual suction which is the water content where large pressures are needed to remove additional soil water. It is interesting to observe that, when suction is close to the residual value, the maximum shear modulus reaches to its maximum value; therefore, it is possible to assume that the air entry value and the residual suction produce the minimum and the maximum shear modulus, respectively, what was also found by Dong & Lu [18].

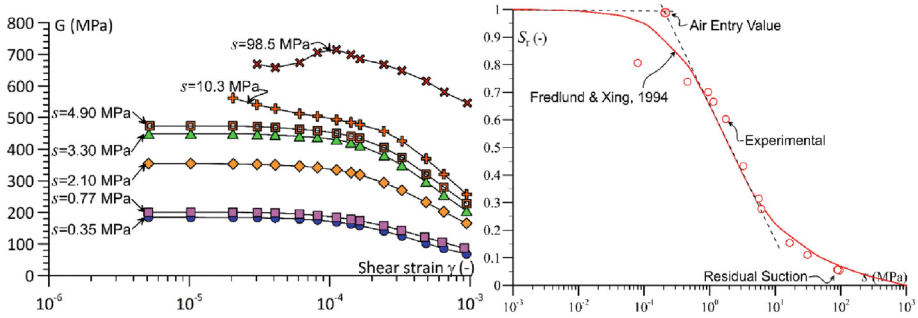


Fig. 1. (left) Shear modulus degradation curves for different suction conditions S of selected soil materials [16] (right) Water retention experimental values and fitting curve proposed by Fredlung & Xing [17]

Fredlung & Xing model used can be described using Eq. (1) and (2) as follows:

$$Sr = C(s) \frac{1}{\left\{ \ln \left(e + \left(\frac{\psi}{a} \right)^n \right) \right\}^m} \tag{1}$$

$$C(s) = 1 - \frac{\ln \left(1 + \frac{\psi}{\psi_{res}} \right)}{\ln \left(1 + \frac{10^6}{\psi_{res}} \right)} \tag{2}$$

where: e is the Neperian base constant

ψ_{res} : suction value at the residual state

ψ : matric suction value corresponding to a particular soil sample saturation degree (S_r).

a, n, m : are experimental parameters obtained (0.95 MPa, 1.04 and 1.50 respectively), while the residual suction S_{res} obtained was 120 MPa.

Fredlung & Xing [17] model with experimental parameters found were implemented in a finite-difference formulation for computing the evolution of saturation within the wall. For this purpose, the mathematical model proposed by Fredlung et al. [19] which is described in Eq. (3) allowed to compute the relative conductivity of the soil k_{rw} , which is also required to compute the evolution of saturation within the wall, using:

$$k_{rw}(s) = \frac{\int_{\ln(s)}^{\ln(10^6)} \frac{\theta(e^y) - \theta(s)}{e^y} \theta'(e^y) dy}{\int_{\ln(s_{av})}^{\ln(10^6)} \frac{\theta(e^y) - \theta_{sat}}{e^y} \theta'(e^y) dy} \tag{3}$$

where $\theta(s)$ is the water retention model proposed by [17], y is the water content corresponding to the analyzed intervals (evenly distributed in the logarithmic space). θ_{sat} : is the water content of the saturated state. θ' : is the first derivative of the model proposed by [17] s_{av} : is the suction for the air entry value for the tested soil. In terms of water content distribution along the walls section, it was assumed that porosity is constant over time. It permits to compute such distribution using an implicit finite difference formulation of Richard's equation, which considers the water flow in the liquid phase, neglecting flow

in the vapor phase. Formulation uses the continuity equation of water flow in unsaturated soils:

$$n \frac{\partial S_r}{\partial t} + \nabla \cdot (-k_w(S_r) \nabla \psi) = 0 \tag{4}$$

which establishes a relationship between the degree of saturation (S_r) over time (t), the soil’s porosity (n), and the divergence of the net water flux which results from the gradient of the total potential (ψ) and the water conductivity of the liquid phase (k_w) as a function of the degree of saturation. The hydraulic conductivity of the liquid phase (k_w) as a function of the degree of saturation is computed multiplying the saturated hydraulic conductivity k_{sat} and the relative permeability $k_{rw}(\theta)$, as described in Eq. (5).

$$k_w = k_{sat} k_{rw}(\theta) \tag{5}$$

A finite-difference formulation using a forward difference time operator and a central difference two-dimensional space operator allows solving the mass conservation equation given in Eq. (4). This procedure allows the discretization in the time and space domains, as in Eqs. (6) and (10), leading to the continuity equation’s discretized form for water flow in unsaturated soil.

$$\nabla \cdot (-k_w(S_r) \nabla \psi) = \frac{k_w^{i,j-\frac{1}{2}}}{\Delta x^2} \psi_{i,j-1} + \frac{k_w^{i,j+\frac{1}{2}}}{\Delta x^2} \psi_{i,j+1} + \frac{k_w^{i-\frac{1}{2},j}}{\Delta y^2} \psi_{i-1,j} + \frac{k_w^{i+\frac{1}{2},j}}{\Delta y^2} \psi_{i+1,j} - \psi_{i,j} \left(\frac{k_w^{i,j-\frac{1}{2}}}{\Delta x^2} + \frac{k_w^{i,j+\frac{1}{2}}}{\Delta x^2} + \frac{k_w^{i-\frac{1}{2},j}}{\Delta y^2} + \frac{k_w^{i+\frac{1}{2},j}}{\Delta y^2} \right) \tag{6}$$

The water conductivity k_w was computed as the geometric mean of the adjacent points of the space discretization. Hence, in Eq. (6), $k_w^{i,j-\frac{1}{2}}$ denotes the geometric mean of the hydraulic conductivity of the nodes row “ i ” column “ j ” and row “ i ” column “ $j-1$ ”; and Δx and Δy are the space discretization of the domain along the “ x ” and “ y ” axes. The “ x ” axis was placed along the thickness modeled rammed earth wall, and the “ y ” axis was placed along with the height of the wall.

The time discretization of the continuity Eq. (4) was developed by establishing a relationship between the saturation degree (S_r) and the total potential (ψ). First, the change of the saturation degree over time was computed in terms of matric suction (s) using Eq. (7), assuming porosity of the material (n) as constant in time. The change of the degree of saturation as a function of suction, known as the water capacity (C_θ), comes from the first derivative of the water retention curve times the porosity (Eq. (8)).

$$n \frac{\partial S_r}{\partial t} = n \frac{\partial S_r}{\partial s} \frac{\partial s}{\partial t} \tag{7}$$

$$n \theta'(s) = C_\theta = n \frac{\partial S_r}{\partial s} \tag{8}$$

Change of suction in time ($\frac{\partial s}{\partial t}$) can be approximated as the change of the total potential in time ($\frac{\partial \psi}{\partial t}$) (Eq. (9)) [19, 20]. This approximation can be adopted because the total potential considers the position’s energy and pore water pressure. However, the

change in position during wetting and drying is negligible compared to the change in pore pressure.

$$\frac{\partial s}{\partial t} = \frac{\partial \psi}{\partial t} \quad (9)$$

The time discretization of the continuity equation was computed using Eqs. (7) to (9). Therefore, the evolution of the total potential for each time step is computed using Eq. (10) as follows:

$$n \frac{\partial S_r}{\partial t} = C_\theta \frac{\partial s}{\partial t} = C_\theta \frac{\psi_{i,j}^{t+\Delta t} - \psi_{i,j}^t}{\Delta t} \quad (10)$$

Calibration of this numerical model used the experimental results from climate chamber's tests, in which wall materials – atmosphere interaction was studied and reported by Lozada et al. [21]. Considering that a key parameter in the soil properties of an earthen wall is the time to reach internal moisture equilibrium during drying, a climatic chamber was designed for measuring soil evaporation rate for a specific set of climate parameters. Lozada et al. experimental program determined the soil water evaporation rates for a compacted soil, using a climatic chamber that allowed to simulate different environmental conditions interacting with soil surfaces. Inside the chamber, wind velocity, solar radiation and relative humidity can be controlled using vents, lamps and cold plate coolers. The equipment permitted to monitor changes of the soil sample's mass due to evaporation causes by the variation of the climate parameters described before. Mass change can be transformed into water flux which was used in the finite-difference simulation of the drying process.

Lozada et al. performed soil water evaporation tests on thin compacted kaolin clay specimens [21]. Evaporation and water flow were obtained in 4 prismatic samples of 0.24 m × 0.24 m and thicknesses of 0.005, 0.01, 0.015 and 0.02 m. The thickest soil specimen was sampled after testing for its gravimetric water content profile. Table 1 shows the atmospheric conditions imposed over during testing, while Fig. 2 shows evaporation flux of the four specimens tested in the chamber. It is possible to observe that evaporation rate is constant at the initial stages due to the high-water availability within the soil. The constant evaporation time limit is denoted as a reference time T_r . For longer times, evaporation rates decrease. The reference time T_r allowed to normalize the four tested sample time scale. Such normalized relationship and the regression (red line in Fig. 2b) was used in this research to compute water flux on the earthen walls boundary conditions during drying. In addition, a linear regression for assessing the reference time at which evaporation starts decaying and the sample thickness H was used (Fig. 2c). Testing of a full scale wall under controlled environmental parameters would have taken around 6 months to reach the residual water content; therefore, the prediction of the reference time using scaled samples is the option. Based on the reduced scale test extrapolation, the reference time for a 0.3 and 0.5 m wide walls was 20.5 and 33.78 h respectively.

As an example of the water content simulation, a comparison between experimental and simulated water content profiles obtained for the 0.02m thick reduced scale model is presented. The numerical simulation intends to identify the wall's water content profile during exposure to dry and wet seasons. The drying process simulation used the water

Table 1. Values of the environmental variables imposed in the climate chamber [21]

Parameter		Value			
Initial soil thickness (mm)		5.2	10.0	14.5	20.5
Dry density (g/cm ³)		1.30	1.31	1.30	1.28
Initial water content (%)		29.5	31.8	31.1	30.0
Irradiance (W/m ²)		860	860	860	860
Air velocity (m/s)	Mean value Std. deviation	$\mu = 1.59$ $\sigma = 0.14$	$\mu = 1.56$ $\sigma = 0.13$	$\mu = 1.48$ $\sigma = 0.10$	$\mu = 1.55$ $\sigma = 0.10$
Air temperature (°C)	Mean value Std. deviation	$\mu = 40.4$ $\sigma = 3.2$	$\mu = 40.9$ $\sigma = 2.1$	$\mu = 42.0$ $\sigma = 1.5$	$\mu = 42.5$ $\sigma = 2.7$
Relative humidity (%)	Mean value Std. deviation	$\mu = 19$ $\sigma = 7$	$\mu = 19$ $\sigma = 4$	$\mu = 18$ $\sigma = 1$	$\mu = 17$ $\sigma = 5$

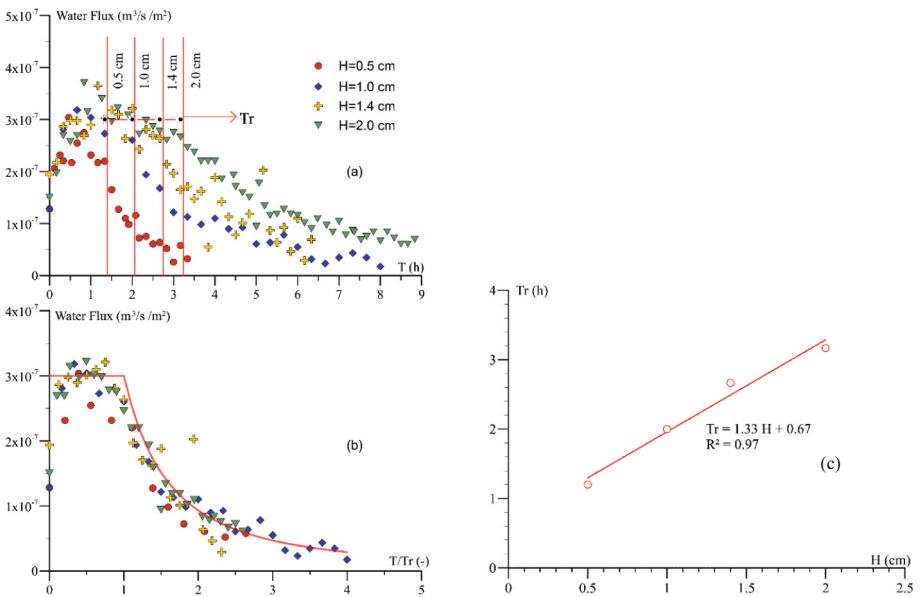


Fig. 2. (a) Evaporation rate in soil specimens. (b) evaporation rate normalized to a reference time Tr. (c) relationship between reference time Tr and wall thickness (H) of the samples during evaporation.

flux measured in the climate chamber as a boundary condition. The evaporation boundary condition identified in the chamber was imposed during the dry season, while imposed potential, corresponding to zero pore pressure, was imposed to simulate wet season. The evaporation simulation initial state was assumed as the potential corresponding to a 86% saturation degree. The wetting simulation initial condition correspond to the end of the drying simulation. The simulation time was 8.3 h, and the water content profile

was computed at the end of the simulation. Figure 3a shows the comparison between the numerical and experimental water content profile. This result allowed to consider that the numerical model can predict the transient evolution of the water content on the two rammed earth structures studied later.

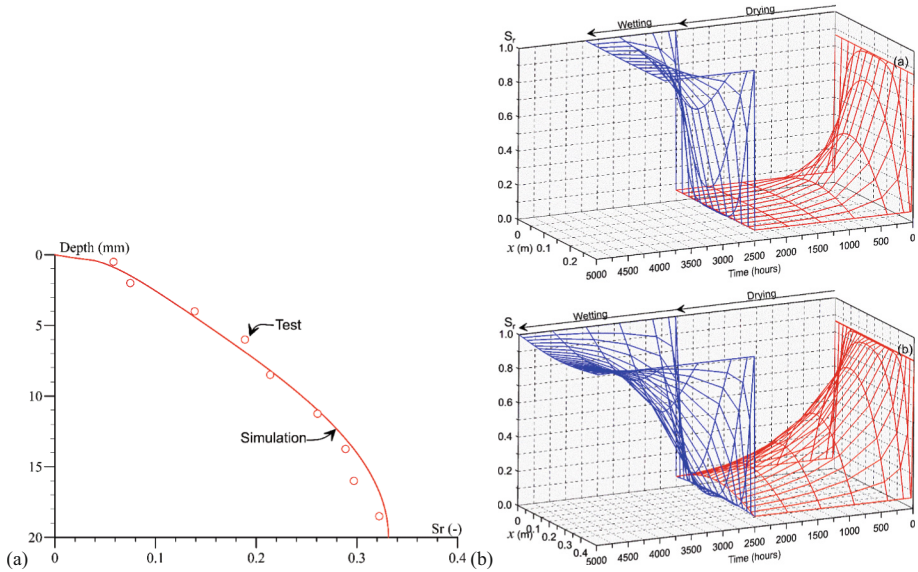


Fig. 3. (a) Comparison between experimental and numerical water content profile for a 0.02 m thick reduced scale specimen. (b) Evolution of soil saturation profile during drying and wetting for a 0.3 m thick wall (upper) and 0.5 m thick wall (lower).

The two earthen walls considered in this study have 2.5 m length and 2.4 m height, and their thicknesses are 0.3 and 0.5 m. In the numerical models, shorter faces are impermeable, whereas, on faces 2.5 by 2.4 m, evaporation or infiltration boundary conditions are imposed. Figure 3b shows saturation degree's evolution within the two simulated walls for different elapsed times. Drying boundary condition was applied for 4333 h; after this drying phase, results show the convergence of water profiles to a value of saturation approaching the compacted material's residual water content. During the wetting process, Fig. 3 shows the faster evolution of the water profiles. For example, the time taken for the 0.3 m wall to reach saturation was 1444 h during the wetting process, compared to the time taken to reach the residual water content 2500 h in the drying simulation. This example evidenced that rammed earth walls can change their mechanical response faster during a wetting process than over an evaporation process. Therefore, for a real structure, it is essential to guarantee correct waterproofing to avoid rapid mechanical changes of the compacted soil.

3 Dynamic Simulation and Walls Seismic Performance

The numerical model described before was implemented in OpenSees using the water content and suction profiles computed as described in the previous section. The Pressure Independent Multi-yield material was assigned to these elements to model the undrained behavior of clays. The modulus reduction curves obtained before were introduced in these materials depending on each point of the wall's water content. The modulus values and the shear modulus reduction curves were linearly interpolated for intermediate values of suction. The natural translational frequency along the strong direction and the modal shape were computed for different times associated with the finite difference simulation's water content profile. Then, Loma Prieta Gilroy N°1 E-W seismic signal was introduced in the model along the wall's length for computing the structural behavior at the initial and residual water content states. Figure 4a shows the first translational mode of vibration along "y" direction, after applying a finite element model having 2400 brick elements (8 nodes – 3 translational degree of freedom) for 0.3 m wall and 4000 brick elements for the 0.5 m wall. Saturation profiles obtained before were used for obtaining mechanical properties in each wall node. The effect of the saturation state on the structural stiffness was reflected as a change in the fundamental frequency. The influence of wall thickness was assessed by comparing the two modeled walls and their fundamental frequency evolution during the wetting and drying process. Figure 4b shows the evolution of the natural frequency during drying and wetting cycles, where it could be seen that the fundamental frequency converges to a constant natural frequency on both drying and wetting. Moreover, the vibration frequency for the evaporation simulation's initial state was similar to the frequency obtained at the end of the wetting simulation. The convergence of the frequencies appeared because at the beginning of the simulation and the end of the wetting and drying processes, the states' water profiles were nearly homogeneous, and shear modulus converged to a constant value when the soil approached either saturation or the residual dry state. The first mode of vibration estimated with the shear beam theory [13, 14] is also compared with the obtained values in Fig. 4. Differences appeared because deformations due to bending and shear are both considered in the simulation.

The Loma Prieta Gilroy N°1 E-W seismic record was used to compute the walls seismic response. This record was selected due to its frequency content and significant amplitude; Fig. 5 (left) shows the acceleration record and its Fast Fourier Transformation (FFT) with a 2.65 Hz predominant frequency, and a PGA of 4.75 m/s². The acceleration at the top face of the walls under the seismic signal was computed for the walls at their extreme wet and dry states, where a homogeneous profile of water content was achieved (i.e., compaction and dry residual states). These states were selected because the natural frequency of vibration converges to two values, one corresponding to the initial or saturated state and the other corresponding to the residual dry water content. Figure 5-middle (a) and (b) shows response accelerations of the 0.3 m thick wall computed for the two extreme conditions, while the FFT spectrum of both responses are showed in Fig. 5-middle (c) and (d). The maximum accelerations obtained were 4.04 m/s² and 1.81 m/s² for the wall having a saturation of 86% and 6%. This response reduction can be attributed to the wall's different stiffness between the wet and the dry states. Figure 5-right shows the same results for the 0.5m thick wall, where the maximum accelerations

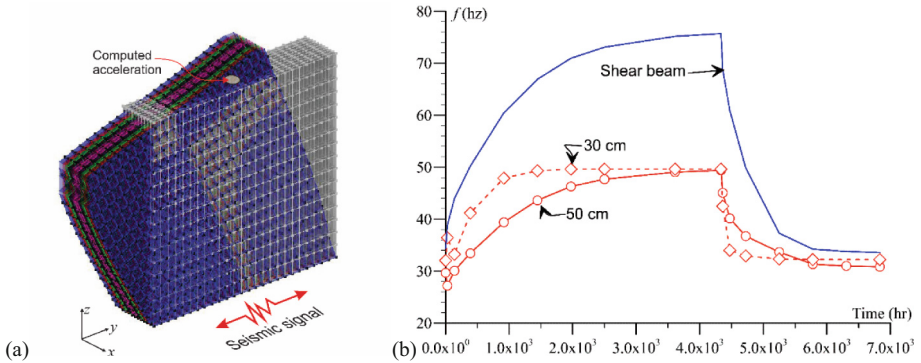


Fig. 4. (a) Translational vibration mode in the “y” in plane direction of the 0.5 m thick modelled wall. (b) Evolution of the translational vibration mode over time of the same wall.

obtained were 3.37 and 1.81 m/s^2 , for the same saturation states. Figure 6 shows the displacement seismic response of both walls under the mentioned saturation states. Results showed again that the structure performed better in dry state than the wet state, reaffirmed the importance of waterproofing once walls reach the residual water content. In addition, it is possible to observe that the wet state models presented permanent deformation after entering in the inelastic range, resulting in permanent damage after the earthquake.

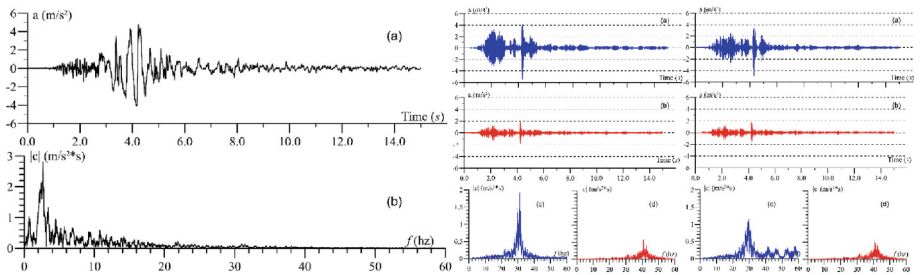


Fig. 5. (left). Loma Prieta Gilroy N°1 E-W seismic record and its FFT, showing a predominant frequency of 2.65 Hz and a PGA of 0.48 g. Figure 5 (right) are the acceleration response of 0.3 m and 0.5 m thick wall in wet (86%, in blue) and dry (6% in red) saturation states and their FFT spectra.

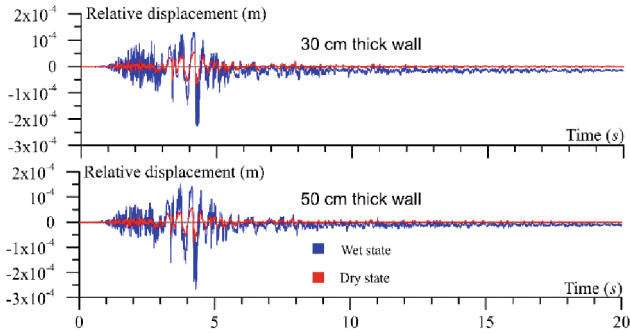


Fig. 6. Displacement seismic response of 0.3 m and 0.5 m thick walls, in wet and dry saturation states under the Loma Prieta Gilroy N°1 E-W seismic record.

4 Conclusions

The influence of environmental conditions on rammed earth structures' seismic behavior was analyzed on two wall geometries with two different thickness (i.e., 2.5 m length by 2.4 m height by 0.3 and 0.5 m thickness). An experimental campaign and numerical simulations were used to achieve the objective. The experimentation phase sought to study the compacted material's hydromechanical properties and establish an evaporation flux when the compacted soil interacts with the environmental conditions. A torsional undrained-unsaturated test was performed on samples at different saturation states for measuring the relationship between maximum shear modulus, shear modulus degradation curves, and suction. A climatic chamber with constant environmental conditions test results were used to measure the soil specimen's water flux. Then, finite difference model results were validated by comparing mathematical estimations against the climatic chamber test results. Values were used to compute water profiles of the modeled walls. Finally, a finite element model was implemented to assess the change in the dynamic properties of the walls and to evaluate their seismic performance.

Results obtained demonstrated mechanical properties dependence on water content. The compacted soil test results showed that the shear modulus increases as matric suction increases (i.e., a reduction of saturation degree within the sample). The maximum shear modulus and suction relation presented a sigmoidal shape related to the soil-water characteristic curve. It was also demonstrated the interaction between environmental conditions and the compacted material. The results showed a constant water flux up to a time when an exponential decrement can be fitted. Besides, the residual water content could be measured under constant environmental conditions. After, the water content profiles were computed through a finite difference approach validated with the environmental test's experimental results. Finally, finite element simulations revealed an increment of the wall's stiffness in dry conditions reflected in the increase of the fundamental frequency of vibration. The frequency increased from 32 Hz to 49 Hz for the 30 cm wall and 30 Hz to 49 Hz for the 50 cm wall. These results led to the subsequent findings when a non-linear dynamic simulation using a strong ground motion register was performed. The walls behave differently under the same seismic event when their water content is close to saturation or residual state. The walls with high water content

have greater seismic demand compared to when they are dry. It means that environmental conditions had a significant influence on the mechanical behavior of earth structures. This aspect could substantially impact the design, construction, reinforcement, or rehabilitation of earth structures in the future. Nowadays, these aspects are not considered in earthquake resistance design, repair, straightening and rehabilitation studies. In terms of heritage buildings, those aspects could have enormous impact, if they are neglected.

This research used a new procedure and equipment that could be implemented in professional practice. The interaction of the structures and environment can be studied using the novel climatic chamber. The mechanical properties can be obtained using a torsional shear rheometer combined with suction measure equipment. This investigation opens new possibilities for future works where the influence of aspect ratios, different environmental conditions at the faces of the walls, or different compacted materials could be studied. Even more, the influence of several dry-wet cycles during the lifetime of the earth structures and the impact on their mechanical behavior could also be part of further similar studies.

Acknowledgments. This research was partially supported by the PoliGrants program of the Universidad San Francisco de Quito.

References

1. Joaquin, P.A., Augarde, C.E., Gerrard, C.M.: Chronological description of the spatial development of rammed earth techniques. *Int. J. Archit. Herit.* **2**(4), 377–400 (2008)
2. Miccoli, L., Müller, U., Fontana, P.: Mechanical behavior of earthen materials: a comparison between earth block masonry, rammed earth and cob. *Constr. Build. Mater.* **61**, 327–339 (2014)
3. Hall, M., Djerbib, Y.: Rammed earth sample production: context, recommendations and consistency. *Constr. Build. Mater.* **18**(4), 281–286 (2004)
4. Hall, M., Djerbib, Y.: Moisture ingress in rammed earth: Part 1—the effect of soil particle-size distribution on the rate of capillary suction. *Constr. Build. Mater.* **18**(4), 269–280 (2004)
5. Fredlund, D.G., Morgenstern, N.R., Widger, R.A.: The shear strength of unsaturated soils. *Can. Geotech. J.* **15**(3), 313–321 (1978)
6. Fredlund, D.G., Xing, A.: Equations for the soil-water characteristic curve. *Can. Geotech. J.* **31**(4), 521–532 (1994)
7. Vanapalli, S.K., Fredlund, D.G., Pufahl, D.E., Clifton, A.W.: Model for the prediction of shear strength with respect to soil suction. *Can. Geotech. J.* **33**(3), 379–392 (1996)
8. Blatz, J.A., Graham, J.: Elastic-plastic modeling of unsaturated soil using results from a new triaxial test with controlled suction. *Géotechnique* **53**(1), 113–122 (2003)
9. François, B., Palazon, L., Gerard, P.: Structural behaviour of unstabilized rammed earth constructions submitted to hygroscopic conditions. *Constr. Build. Mater.* **155**, 164–175 (2017)
10. Bui Bui, Q.B., Morel, J.C., Reddy, B.V., Ghayad, W.: Durability of rammed earth walls exposed for 20 years to natural weathering. *Build. Environ.* **44**(5), 912–919 (2009)
11. Bui Bui, Q.B., Morel, J.C., Hans, S., Meunier, N.: Compression behaviour of non-industrial materials in civil engineering by three scale experiments: the case of rammed earth. *Mater. Struct.* **42**(8), 1101–1116 (2009)
12. Bui Bui, Q.B., Hans, S., Morel, J.C., Do, A.P.: First exploratory study on dynamic characteristics of rammed earth buildings. *Eng. Struct.* **33**(12), 3690–3695 (2011)

13. Bui Bui, Q.B., Bui, T.T., Limam, A.: Assessing the seismic performance of rammed earth walls by using discrete elements. *Cogent Eng.* **3**(1), 1200835 (2016)
14. Bui, T.-T., Bui, Q.-B., Limam, A., Morel, J.-C.: Modeling rammed earth wall using discrete element method. *Continuum Mech. Thermodyn.* **28**(1–2), 523–538 (2015). <https://doi.org/10.1007/s00161-015-0460-3>
15. El El-Nabouch, R., Bui, Q.B., Ple, O., Perrotin, P.: Assessing the in-plane seismic performance of rammed earth walls by using horizontal loading tests. *Eng. Struct.* **145**, 153–161 (2017)
16. Villacreses, J.P., Caicedo, B., Caro, S., Yépez, F.: A novel procedure to determine shear dynamic modulus and damping ratio for partial saturated compacted fine-grained soils. *Soil Dyn. Earthq. Eng.* **131**, 106029 (2020)
17. Dong, Y., Lu, N.: Dependencies of shear wave velocity and shear modulus of soil on saturation. *J. Eng. Mech.* **142**(11), 04016083 (2016)
18. Fredlund, D.G., Xing, A., Huang, S.: Predicting the permeability function for unsaturated soils using the soil-water characteristic curve. *Can. Geotech. J.* **31**(4), 533–546 (1994)
19. Caicedo, B.: *Geotechnics of Roads: Fundamentals*, 1st edn. CRC Press, London (2018)
20. Caicedo, B.: *Geotechnics of Roads: Advanced Analysis and Modelling*, 1st edn. CRC Press, London (2021)
21. Lozada, C., Caicedo, B., Thorel, L.: A new climatic chamber for studying soil–atmosphere interaction in physical models. *Int. J. Phys. Model. Geotech.* **19**(6), 286–304 (2019)